Microscopic positive-energy potential based on the Gogny interaction

G. Blanchon,[1,*] M. Dupuis,[1] H. F. Arellano,[1,2] and N. Vinh Mau[1]

[1]*CEA, DAM, DIF F-91297 Arpajon, France*

[2]*Department of Physics - FCFM, University of Chile, Av. Blanco Encalada 2008, Santiago, Chile*

We present a nucleon elastic scattering calculation based on Green's function formalism in the random-phase approximation. For the first time, the finite-range Gogny effective interaction is used consistently throughout the whole calculation to account for the complex, nonlocal, and energy-dependent optical potential. Effects of intermediate single-particle resonances are included and found to play a crucial role in the account for measured reaction cross sections. Double counting of the particle-hole second-order contribution is carefully addressed. The resulting integro-differential Schrödinger equation for the scattering process is solved without localization procedures. The method is applied to neutron and proton elastic scattering from ^{40}Ca. A successful account for differential and integral cross sections, including analyzing powers, is obtained for incident energies up to 30 MeV. Discrepancies at higher energies are related to a much-too-high volume integral of the real potential for large partial waves. This work opens the way to simultaneously assess effective interactions suitable for both nuclear structure and reactions.

PACS number(s): 24.10.Cn, 21.30.Fe, 24.10.Ht, 25.40.Cm

I. INTRODUCTION

Several elements are required to perform nuclear reaction cross-section calculations: the optical model potential, the nuclear level densities, the γ-ray strength functions, and the fission properties. Those models are gathered into robust and well-tested nuclear reaction codes, such as TALYS [1] or EMPIRE [2]. They mostly rely on parameters usually adjusted to experimental data. On the other hand, a large amount of nuclear data is needed for assessment and predictions for rare-isotopes facilities, for r processes, and for advanced reactor applications. As a result, nuclear reaction cross sections are unavoidably extrapolated from the domain where phenomenological models have been tested.

Along this line a coherent theoretical model to describe both static properties as well as collisions observables becomes the sole practical means to provide a systematic description of cross-section data. Nuclear-matter-folding models have led to reasonable descriptions of nucleon elastic scattering at incident energies above $\sim$50 MeV, even up to $\sim$1.5 GeV [3,4]. Although *ab initio* methods have made progress [5–11] in handling light and magic nuclei, they are still not suited for heavy targets nor for high-incident-energy projectiles.

Among microscopic structure models, methods based on energy-density functionals emerge as a promising tractable theoretical tool that can be applied to all the nuclides with $A \gtrsim 40$. Self-consistent mean-field theory and its extensions beyond mean field have proven to be well suited to describe open-shell nuclei, where pairing correlations and deformation effects play an important role. These approaches have successfully predicted a broad body of nuclear structure data for medium- to heavy-mass nuclei. Recent works have aimed to extend this wealth of developments to reaction calculations through coupled-channel calculations with mean-field inputs [12], or continuum particle-vibration coupling using

a Skyrme effective nucleon-nucleon (NN) interaction [13]. Other approaches are in progress, where an optical potential is approximated as the Hartree–Fock (HF) term plus the imaginary part of the uncorrelated particle-hole potential neglecting the collectivity of target excited states [14,15].

In this work we use the so-called nuclear structure method (NSM) for scattering [16–20] based on the self-consistent HF and random-phase approximations (RPA) of the microscopic optical potential. Special attention is given to the issue of the double counting of the second-order diagram, which has not been addressed in previous works [12,13]. We show that the subtraction of the second-order term does not lead to pathological behaviors when positive incident energy is considered, contrary to what is expected in Ref. [21]. Moreover, we use the finite-range Gogny effective interaction [22], which is suitable for the discussions of second-order effects and does not suffer the need of an *ad hoc* momentum cutoff as do Skyrme interactions [23]. This interaction is used consistently throughout the whole calculation. Careful treatment of these different aspects allows us to describe scattering observables at a good level of accuracy which could not be achieved in previous implementations of NSM. These calculations have been made possible thanks to modern calculation capabilities.

II. METHOD

In NSM [16], the optical potential V consists of two components,

$$V = V^{HF} + \Delta V. \qquad (1)$$

The HF potential, V^{HF}, is the major contribution to the real part of the optical potential. V^{HF} is calculated in coordinate space to ensure the correct asymptotic behavior of single-particle states. It is nonlocal and energy independent due to the nature of the Gogny interaction, which is of finite range and energy independent, respectively. Rearrangement contributions stemming from the density-dependent term of the interaction are also taken into account.

*Corresponding author: guillaume.blanchon@cea.fr

The second component of the potential in Eq. (1) is

$$\Delta V = V^{PP} + V^{RPA} - 2V^{(2)}, \qquad (2)$$

which is complex, energy dependent, and nonlocal. Here V^{PP} and V^{RPA} are contributions from particle-particle and particle-hole correlations, respectively. The uncorrelated particle-hole contribution $V^{(2)}$ is accounted for once in V^{PP} and twice in V^{RPA}. As a matter of fact, if two-body correlations are neglected in Eq. (2) for V^{PP} and V^{RPA}, then ΔV reduces to $V^{(2)}$, as expected [16].

As mentioned in Ref. [19], if one works with a NN effective interaction with a density-dependent term, such as Gogny or Skyrme forces, attention must be paid to correlations already accounted for in the interaction. Indeed, part of the particle-particle correlations is already contained at the HF level as far as Re[V^{PP}] is concerned. We thus use the same prescription as in Ref. [18], omitting Re[V^{PP}] while Im[V^{PP}] is approximated by Im[$V^{(2)}$]. Then Eq. (2) becomes

$$\Delta V = \text{Im}[V^{(2)}] + V^{RPA} - 2V^{(2)}. \qquad (3)$$

From now on, equations are presented omitting spin for simplicity. For nucleons with incident energy E, the RPA potential reads

$$V^{RPA}(\mathbf{r}, \mathbf{r}', E) = \sum_{N \neq 0} \sum_{\lambda} \left[\frac{n_\lambda}{E - \varepsilon_\lambda + E_N - i\Gamma(E_N)} \right.$$
$$+ \frac{1 - n_\lambda}{E - \varepsilon_\lambda - E_N + i\Gamma(E_N)} \bigg]$$
$$\times \Omega_\lambda^N(\mathbf{r}) \Omega_\lambda^N(\mathbf{r}'), \qquad (4)$$

where n_i and ε_i are the occupation number and energy of the single-particle state ϕ_i in the HF field, respectively. Subscripts p, h, and λ refer to the quantum number of the particle, hole, and intermediate single-particle, respectively. E_N and $\Gamma(E_N)$ represent the energy and the width of the Nth excited state of the target, respectively. Additionally,

$$\Omega_\lambda^N(\mathbf{r}) = \sum_{(p,h)} [X^{N,(p,h)} F_{ph\lambda}(\mathbf{r}) + Y^{N,(p,h)} F_{hp\lambda}(\mathbf{r})], \qquad (5)$$

where X and Y denote the usual RPA amplitudes and

$$F_{ij\lambda}(\mathbf{r}) = \int d^3\mathbf{r}_1 \phi_i^*(\mathbf{r}_1) v(\mathbf{r}, \mathbf{r}_1)[1 - \hat{P}] \phi_\lambda(\mathbf{r}) \phi_j(\mathbf{r}_1), \qquad (6)$$

where $\hat{P}$ is a particle-exchange operator and v is the NN effective interaction. The particle-hole contribution reads

$$V^{(2)}(\mathbf{r}, \mathbf{r}', E) = \frac{1}{2} \sum_{ij} \sum_{\lambda} \left[\frac{n_i(1 - n_j)n_\lambda}{E - \varepsilon_\lambda + E_{ij} - i\Gamma(E_{ij})} \right.$$
$$+ \frac{n_j(1 - n_i)(1 - n_\lambda)}{E - \varepsilon_\lambda - E_{ij} + i\Gamma(E_{ij})} \bigg]$$
$$\times F_{ij\lambda}(\mathbf{r}) F_{ij\lambda}^*(\mathbf{r}'), \qquad (7)$$

with $E_{ij} = \varepsilon_i - \varepsilon_j$ being the uncorrelated particle-hole energy.

The description of target excitations has been obtained by solving the RPA/D1S equations in a harmonic oscillator basis, including fifteen major shells [24] and using the D1S

Gogny interaction [22]. We account for RPA excited states with spin up to $J = 8$, including both parities in order to achieve convergence of the cross section. The first 1^- state given by RPA, containing the translational spurious mode, is removed. In order to avoid spurious modes in the uncorrelated particle-hole term, we approximate the 1^- contribution in $V^{(2)}$ by half that of the 1^- contribution in V^{RPA}. Coupling to excited states results in a number of poles in Eqs. (4) and (7). Moreover, fluctuations appear in the imaginary part of the potential whenever the energy $E - E_N$ matches a resonance energy of the intermediate single-particle state ϕ_λ. Inclusion of single-particle resonances is made possible thanks to the HF potential in coordinate space and to the correct treatment of the continuum. The leading inelastic doorways are those containing single-particle resonances. These contributions lead to significant enhancement of the reaction cross section compared with the calculation where ϕ_λ are approximated with plane waves. Although the RPA/D1S method provides a good overall description of the spectroscopic properties of double-closed-shell nuclei, couplings to two or more particle-hole states and to continuum states are neglected. The impact of these couplings is a strength redistribution that can be handled assigning a finite width $\Gamma(E_N)$ to each RPA state. It has the effect of averaging in energy and smoothing the potential. The resulting potential can then be identified with an optical model [25]. A microscopic calculation of these widths is beyond the scope of the present study. We include them phenomenologically as an interpolation between reasonable values. $\Gamma(E_N)$ takes the value of 2, 5, 15, and 50 MeV for excitation energies of 20, 50, 100, and 200 MeV, respectively. The specific choice of the width parametrization does not affect our predictions. The integro-differential Schrödinger equation for elastic scattering is solved, retaining the nonlocal structure of the potential [26]. Moreover, optical potential calculations yield shape-elastic, reaction, and total cross sections [25]. The compound-elastic cross section has to be added to the shape-elastic cross section and subtracted from the reaction cross section before comparison with data [25]. In a first attempt, we use the compound-elastic contribution from Hauser–Feshbach calculations with the TALYS code [1] using the Koning–Delaroche global potential [27]. These considerations are particularly relevant for neutron scattering below 10 MeV.

III. RESULTS

In Fig. 1, we present results for the calculated differential cross sections based on NSM for both neutron and proton scattering from ^{40}Ca. References to data are given in Ref. [27]. Error bars are smaller than the size of the symbols. NSM results compare very well to experiment and those based on the Koning–Delaroche potential up to about 30 MeV incident energy. Beyond 30 MeV, backward-angle cross sections are overestimated. Discrepancies at 16.9 MeV (23.5 MeV) for neutron (proton) scattering are related to resonances in the intermediate single-particle state when not completely averaged. A detailed treatment of the width might cure this issue. In Fig. 2 we show calculated analyzing powers for neutron and proton scattering at several energies, in good agreement with measurements. Moreover, agreement with the data is
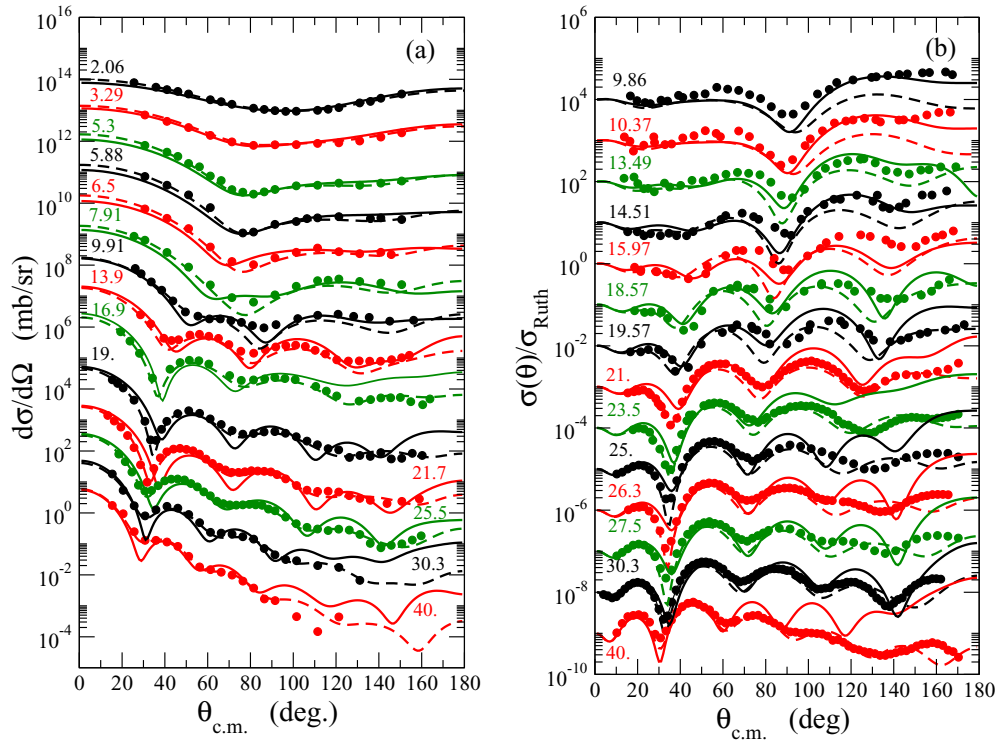
FIG. 1. (Color online) Differential cross sections for (a) neutron and (b) proton scattering from ^{40}Ca. Comparison is between data (symbols), $V^{HF} + \Delta V$ results (solid curves), and Koning–Delaroche potential results (dashed curves).

comparable to that obtained from the Koning–Delaroche potential. These results suggest that the NSM potential retains the correct spin-orbit behavior. In Fig. 3 we show reaction cross section for proton scattering [Fig. 3(a)] and total cross section for neutron scattering [Fig. 3(b)]. Calculated reaction cross sections are in good agreement with experiments. For neutrons, however, we underestimate the total cross section

below 10 MeV. Considering that the differential elastic cross section is well reproduced, this underestimate suggests that part of the absorption mechanism is not accounted for, such as target-excited states beyond RPA or double-charge exchange processes.

To understand the limited energy range of applicability of the NSM approach, we compare in Fig. 4 the volume integral
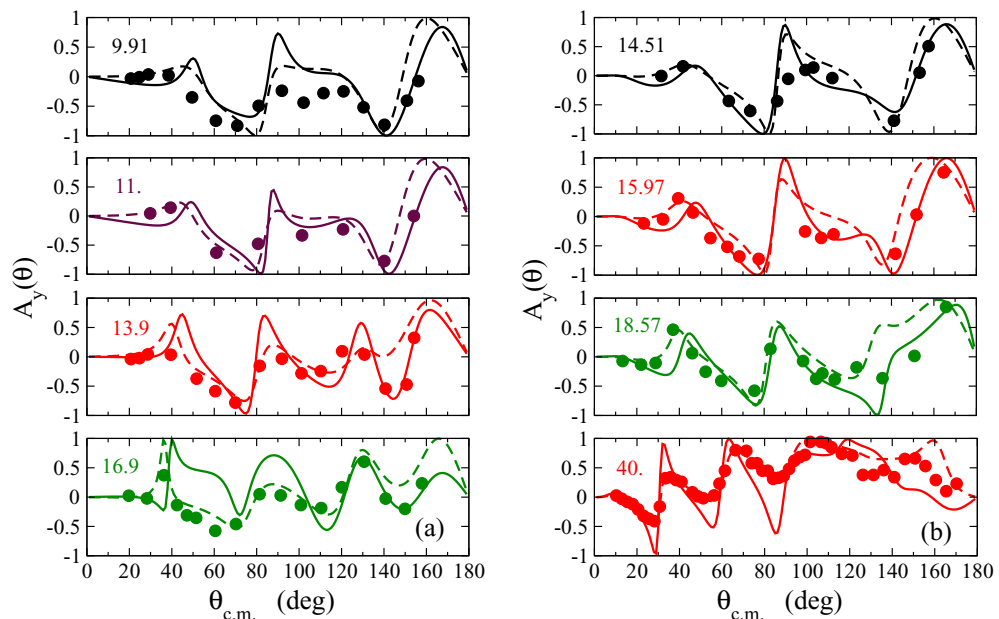

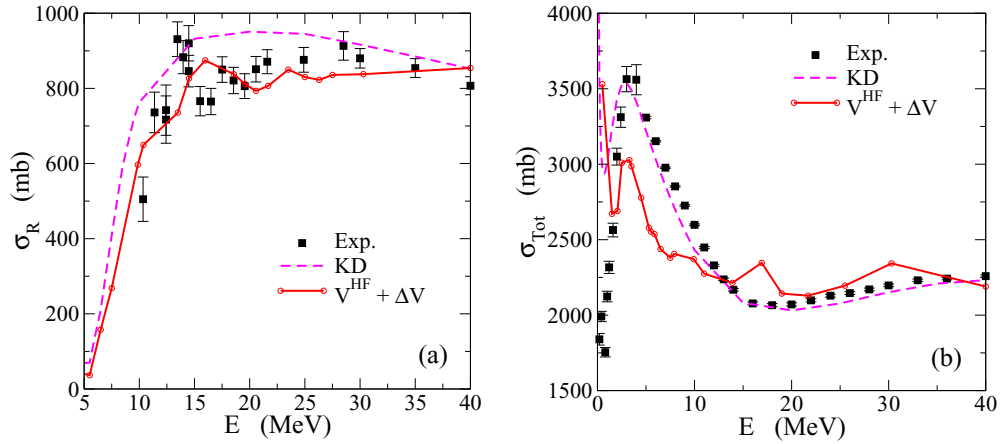FIG. 2. (Color online) Same as Fig. 1 but for analyzing powers.

FIG. 3. (Color online) Reaction cross section for (a) proton and (b) total cross section for neutron scattering from ^{40}Ca. Comparison is between data (symbols), $V^{HF} + \Delta V$ results (solid curve), and Koning–Delaroche potential (dashed curve).

J_V of the central HF potential with that obtained from the real part of the Perey–Buck nonlocal potential [28]. Black segments denote the strongest partial-wave contributions accounting for 80% of the reaction cross section at the selected incident energies. Keep in mind that the HF potential is the leading contribution to the real part of V in Eq. (1). Its contribution to J_V is similar to that from Perey–Buck up to about the twelfth partial wave ($\sim$17 MeV). Beyond this point, HF saturates, following the trend of the Hartree potential which is local and thus partial-wave independent. This departure from Perey–Buck explains why increasing incident energy (partial wave) yields much-too-high J_V for HF, with the subsequent

overestimate of the differential cross section at backward angles. It would be interesting to investigate to what extent the effective interaction has incidence on this behavior at high partial wave.

We now address the subtraction of the uncorrelated second-order term in Eq. (2). As pointed out in Ref. [21], this subtraction can lead to unphysical solutions with spurious poles and negative occupation numbers. The smooth and averaged potential obtained from Eq. (1) no longer suffers these pathologies. Indeed, if one approximates $V^{(2)} \approx V^{RPA}/2$, then Eq. (2) reduces to

$$\Delta V \approx \text{Im}[V^{RPA}/2]. \qquad (8)$$

This approximation has the drawback of neglecting the real part of ΔV as well as part of the collectivity of the excited states. However, it has the advantage of avoiding second-order
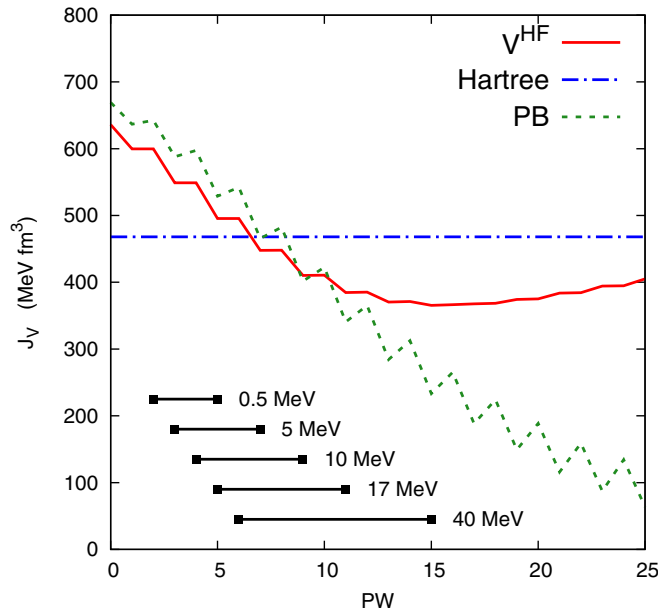

FIG. 4. (Color online) Volume integral as a function of partial waves for neutron scattering from ^{40}Ca: HF potential (solid curve), Hartree potential (dash-dotted curve), and Perey–Buck potential (dotted curve). Horizontal segments denote the partial-wave interval to sum up 80% of the reaction cross section at selected incident energies.
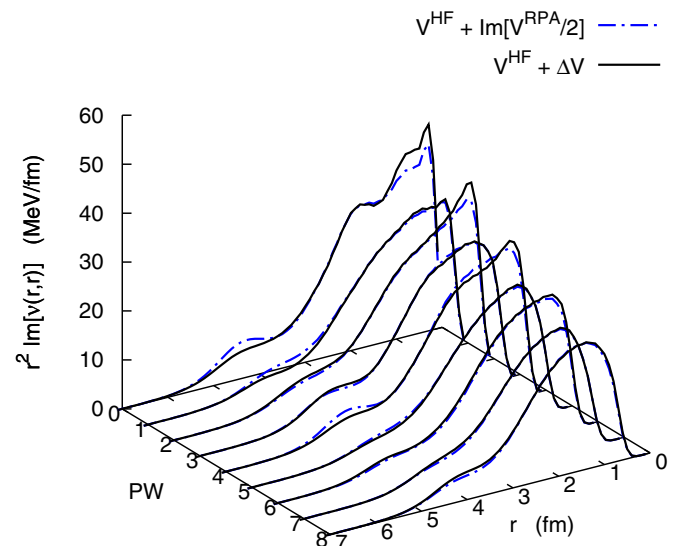

FIG. 5. (Color online) Partial-wave contribution ν of ImV for neutron scattering from ^{40}Ca scattering at 9.91 MeV as a function of radius and partial waves: $V^{HF} + \Delta V$ potential (solid curve), $V^{HF} + \text{Im}[V^{RPA}/2]$ potential (dash-dotted curve).
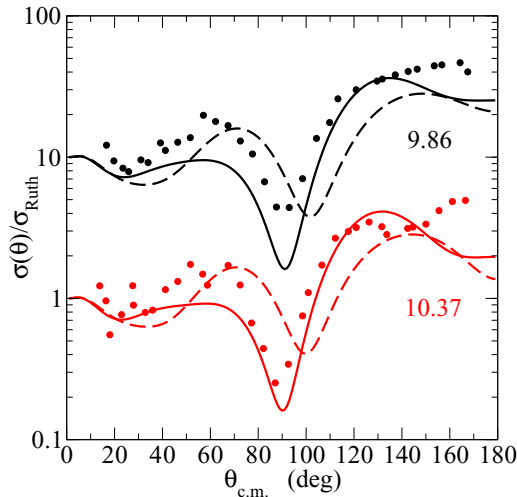
FIG. 6. (Color online) Differential cross sections $\sigma(\theta)/\sigma_{\mathrm{Ruth}}$ for proton incident on ^{40}Ca. Comparison between data (symbols), $V^{HF} + \Delta V$ (solid curves), and $V^{HF} + \mathrm{Im}[V^{RPA}/2]$ results (dashed curves).

double counting. As seen in Fig. 5, both approximations in Eqs. (3) and (8) yield very similar shapes for each partial-wave contribution ν of the diagonal imaginary part of $\mathrm{Im}[V]$ for neutron scattering from ^{40}Ca at 9.91 MeV. This trend remains true for higher partial waves and incident energies, confirming the good behavior of $V^{HF} + \Delta V$. In Fig. 6 we present the differential cross section for proton scattering from ^{40}Ca based

on these two approximations. The diffractive minima obtained with $V^{HF} + \Delta V$ agree better with experiment than those obtained from $V^{HF} + \mathrm{Im}[V^{RPA}/2]$. This result emphasizes the important role played by the real part of ΔV.

IV. CONCLUSION

The work presented here constitutes a promising step forward aimed to a model keeping at the same footing both reaction and structure aspects of the many-nucleon system. Within the optical model potential, NSM is able to account reasonably well for low-energy-scattering data. An important feature of the approach is the extraction of the imaginary part of the potential by means of intermediate excitations of the system. It has been based on the Gogny effective interaction, although it can be applied to any interaction of similar nature. The study has been restricted to a closed-shell target but can be extended to account for pairing correlations as well as axial deformation using quasiparticle RPA. Those results also open the way to new parametrizations of NN effective interactions including reaction constraints. A comprehensive work on the formalism and applications shall be presented elsewhere.

[1] A. J. Koning, S. Hilaire, and M. Duijvestijn, in *Proceeding of the International Conference on Nuclear Data for Science and Technology-ND2007* (EDP Sciences, Paris, 2008), pp. 211–214.

[2] M. Herman, R. Capote, B. V. Carlson, P. Obložinský, M. Sin, A. Trkov, H. Wienke, and V. Zerkin, Nucl. Data Sheets **108**, 2655 (2007).

[3] M. Dupuis, S. Karataglidis, E. Bauge, J. P. Delaroche, and D. Gogny, Phys. Rev. C **73**, 014605 (2006).

[4] H. F. Arellano and H. V. von Geramb, Phys. Rev. C **66**, 024602 (2002).

[5] S. Quaglioni and P. Navrátil, Phys. Rev. Lett. **101**, 092501 (2008).

[6] G. Hupin, J. Langhammer, P. Navrátil, S. Quaglioni, A. Calci, and R. Roth, Phys. Rev. C **88**, 054622 (2013).

[7] K. M. Nollett, S. C. Pieper, R. B. Wiringa, J. Carlson, and G. M. Hale, Phys. Rev. Lett. **99**, 022502 (2007).

[8] H. Dussan, S. J. Waldecker, W. H. Dickhoff, H. Müther, and A. Polls, Phys. Rev. C **84**, 044319 (2011).

[9] G. Hagen and N. Michel, Phys. Rev. C **86**, 021602 (2012).

[10] V. Somà, C. Barbieri, and T. Duguet, Phys. Rev. C **87**, 011303 (2013).

[11] V. Somà, C. Barbieri, and T. Duguet, Phys. Rev. C **89**, 024323 (2014).

[12] G. P. A. Nobre, F. S. Dietrich, J. E. Escher, I. J. Thompson, M. Dupuis, J. Terasaki, and J. Engel, Phys. Rev. Lett. **105**, 202502 (2010).

[13] K. Mizuyama and K. Ogata, Phys. Rev. C **86**, 041603 (2012).

[14] V. V. Pilipenko and V. I. Kuprikov, Phys. Rev. C **86**, 064613 (2012).

[15] Y. Xu, H. Guo, Y. Han, and Q. Shen, J. Phys. G **41**, 015101 (2014).

[16] N. Vinh Mau, *Theory of Nuclear Structure* (IAEA, Vienna, 1970), p. 931.

[17] N. Vinh Mau and A. Bouyssy, Nucl. Phys. A **257**, 189 (1976).

[18] V. Bernard and N. Van Giai, Nucl. Phys. A **327**, 397 (1979).

[19] A. Bouyssy, H. Ngô, and N. Vinh Mau, Nucl. Phys. A **371**, 173 (1981).

[20] F. Osterfeld, J. Wambach, and V. A. Madsen, Phys. Rev. C **23**, 179 (1981).

[21] C. Barbieri and W. H. Dickhoff, Phys. Rev. C **63**, 034313 (2001).

[22] J. F. Berger, M. Girod, and D. Gogny, Comput. Phys. Commun. **63**, 365 (1991).

[23] T. Skyrme, Nucl. Phys. **9**, 615 (1959).

[24] J. Blaizot and D. Gogny, Nucl. Phys. A **284**, 429 (1977).

[25] H. Feshbach, Ann. Phys. (NY) **5**, 357 (1958).

[26] J. Raynal, computer code DWBA98, NEA 1209/05 (1998).

[27] A. J. Koning and J. P. Delaroche, Nucl. Phys. A **713**, 231 (2003).

[28] F. Perey and B. Buck, Nucl. Phys. **32**, 353 (1962).